Optics Letters

Essential differences between TE and TM band gaps in periodic films at the first Bragg condition

Sun-Goo Lee and Robert Magnusson*

Department of Electrical Engineering, University of Texas at Arlington, Arlington, Texas 76019, USA
**Corresponding author: magnusson@uta.edu*

Received 29 July 2019; revised 25 August 2019; accepted 27 August 2019; posted 27 August 2019 (Doc. ID 374079); published 18 September 2019

In photonic lattices with thin-film geometry, TE modes possess an in-plane electric field component parallel to the film surface, whereas TM modes have a magnetic field component similarly oriented. This study reports the essential properties of, and differences between, TE and TM band gaps induced by laterally periodic thin-film photonic lattices at the first Bragg condition. Because TE and TM guided waves obey different wave equations, TE and TM band gaps exhibit different evolution as the film thickness varies. The first TM band exhibits both band gap closure and band flips wherein the symmetry properties of the band-edge modes are reversed by variation of film thickness. In the first TE band, in contrast, there is neither band gap closure nor band flip. The work provides an insightful semianalytical formulation whose results are verified by rigorous computations.

https://doi.org/10.1364/OL.44.004658

Thin-film photonic lattices and metastructures possessing photonic band gaps are of interest due to their ability to manipulate light propagation and localization at subwavelength scales. Various photonic devices such as waveguides [1,2], lasers [3,4], wide-band reflectors [5], and filters [6] are realized based on photonic band gaps of periodic photonic lattices with one-dimensional (1D) or two-dimensional (2D) refractive index modulation. Thin-film photonic lattices are attractive because they allow both nonleaky and leaky stop bands [7]. Nonleaky band gaps are useful in controlling the flow of light inside slab structures [8], and leaky stop bands are associated with diverse spectral responses generated by lateral guided-mode resonances [9,10]. Moreover, guided waves in thin-film photonic lattices are classified into two categories by their polarization directions. A TE mode is described by electric field components parallel to the film and a TM mode by parallel magnetic field components [11]. Hence, diverse polarization-dependent photonic devices are feasible because the position and size of TE and TM band gaps are different in general.

The purpose of this Letter is to introduce and analyze the fundamentally different properties of TE and TM band gaps in thin-film photonic lattices. In ideal 1D photonic lattices with infinite lateral extent (~Bragg stacks) under broadside normal incidence, TE and TM band gaps are not distinguishable because TE and TM modes are perfectly degenerate. In periodic thin-film photonic lattices with finite thickness, however, TE and TM modes are distinct. We show herein that the TE and TM band gaps undergo dissimilar evolution as the film thickness varies. The first TM band exhibits band gap closure and a band flip, wherein the symmetry properties of band edge modes are converted by the variation of thin-film thickness. The TE band, in contrast, has neither a band gap closure nor a band flip. To understand the properties of the TE and TM bands, we employ a semianalytical dispersion model and finite-difference time-domain (FDTD) simulations [12].

As shown in Fig. 1, for simplicity and clarity, we model a 1D photonic lattice of alternating media with high (ε_h) and low (ε_l) dielectric constants. The width of the high-dielectric-constant part is $\rho\Lambda$, where Λ is the period, and the lattice thickness is d. The photonic lattice supports both TE and TM guided modes via total internal reflection because its average dielectric constant $\varepsilon_{\text{avg}} = \varepsilon_l + \rho(\varepsilon_h - \varepsilon_l)$ exceeds that of the surrounding medium ε_s. As represented in Fig. 1, the TE (TM) mode has an in-plane electric (magnetic) field component parallel to the film surface and propagates along the z direction. Photonic band gaps open for both TE and TM modes when $\Delta\varepsilon = \varepsilon_h - \varepsilon_l > 0$ and $0 < \rho < 1$. In general, if the lattice supports numerous guided modes, each mode can have multiple band gaps at the Bragg condition $k_z = q\text{K}/2$ where k_z is the modal wavenumber, $\text{K} = 2\pi/\Lambda$ is the magnitude of the grating vector, and q is an integer denoting the Bragg order [13]. In this Letter, we focus on the nonleaky first band ($q = 1$) of the fundamental TE_0 and TM_0 modes because this simple case clearly shows the essential difference between the TE and TM band gaps under variation of film thickness d.

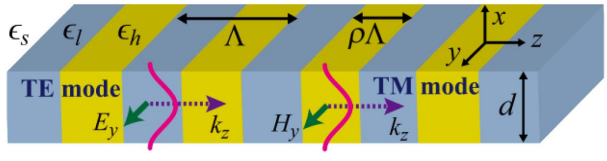

Fig. 1. Model of a 1D photonic lattice with finite thickness d in the x direction and with infinite lateral extent in the y and z directions. The first TE and TM band gaps open at $k_z = \pi/\Lambda$.

Figures 2(a) and 2(b) show the evolution of the first TE and TM band gaps, respectively, under variation of thickness d. As seen in Fig. 2(a), the first TM band gap opens at $k_z/\mathrm{K} = 0.5$, and its size increases as d increases from zero. As the thickness further increases, however, the gap size decreases and becomes zero when $d = 0.82\Lambda$. The TM band gap reopens and widens on additional increase in d. Band flip is seen clearly by the spatial magnetic field profiles of band edge modes plotted in the insets of Fig. 2(a). Spatial field distributions are calculated at the $y = 0$ plane, and vertical dotted lines represent the mirror plane, the center of the high dielectric constant part, in the computational cells. When the thickness is 0.20Λ and 0.60Λ, the upper and lower band edge modes have asymmetric and symmetric magnetic field (H_y) distributions according to the mirror plane, respectively. With $d = 0.82\Lambda$, the TM band gap closes and band edge modes degenerate. When $d = 0.90\Lambda$ and $d = 1.10\Lambda$, the field profiles are reversed and the upper (lower) band edge modes have symmetric (asymmetric) field distributions. As shown in Fig. 2(b), the TE band gap also opens and its size increases with d. However, the gap size slowly decreases by additional increase in d. The insets of Fig. 2(b) show that the upper and lower band edge modes have asymmetric and symmetric spatial electric field (E_y) distributions, respectively, irrespective of d. In the case of the TE mode, unlike the TM mode, there is no band closure and no band flip induced by variation of film thickness. Incidentally, Fig. 2 also shows that the frequency positions of the TE and TM band gaps downshift as d increases because the effective indices of the guided modes increase when d increases. However, we focus our attention on the evolution of the band structure and on the change in the symmetry properties of the band edge modes under variation of film thickness.

To understand the physical origin of the different evolution of the TE and TM band gaps shown in Fig. 2, we investigate the photonic band structures by solving the wave equations for TE mode with E_y and TM mode with H_y given by

$$\frac{\partial^2 E_y}{\partial x^2} + \frac{\partial^2 E_y}{\partial z^2} + \varepsilon k_0^2 E_y = 0, \tag{1}$$

$$\frac{\partial}{\partial x}\left(\xi \frac{\partial H_y}{\partial x}\right) + \frac{\partial}{\partial z}\left(\xi \frac{\partial H_y}{\partial z}\right) + k_0^2 H_y = 0, \tag{2}$$

where $\xi = 1/\varepsilon$ is the inverse of the dielectric function [14,15]. To solve Eqs. (1) and (2), we use a semianalytical dispersion model in which the electric and magnetic field distributions for TE and TM modes are approximated as

$$E_y(x,z) \approx [A(z)e^{+i\mathrm{X}z} + B(z)e^{-i\mathrm{X}z}]\varphi_{\mathrm{TE}}(x), \tag{3}$$

$$H_y(x,z) \approx [A(z)e^{+i\mathrm{X}z} + B(z)e^{-i\mathrm{X}z}]\varphi_{\mathrm{TM}}(x), \tag{4}$$

respectively, where $\mathrm{X} = 0.5$ K, $\varphi_{\mathrm{TE}}(x)$ and $\varphi_{\mathrm{TM}}(x)$ represent the transverse TE and TM mode profiles of the unmodulated waveguide, respectively, and $A(z)$ and $B(z)$ are slowly varying envelopes of two counter-propagating waves characteristic of such lattices. The dielectric function $\varepsilon(x,z)$ and its inverse $\xi(x,z)$ are expanded as Fourier series, and we consider only the zeroth and first-order Fourier harmonics such that

$$\varepsilon(x,z) \approx \varepsilon_0(x) + \varepsilon_1(x)\cos(\mathrm{K}z), \tag{5}$$

$$\xi(x,z) \approx \xi_0(x) + \xi_1(x)\cos(\mathrm{K}z), \tag{6}$$

where $\varepsilon_0(x) = \varepsilon_{\mathrm{avg}}$, $\varepsilon_1(x) = (2\Delta\varepsilon/\pi) \times \sin(\pi\rho)$, $\xi_0(x) = \rho/\varepsilon_h + (1-\rho)/\varepsilon_l$, and $\xi_1(x) = -(2\Delta\varepsilon/\varepsilon_h\varepsilon_l\pi) \times \sin(\pi\rho)$ when $x \in [-d, 0]$ and $\varepsilon_0(x) = \xi_0(x) = 1$ and $\varepsilon_1(x) = \xi_1(x) = 1$ when $x \notin [-d, 0]$. The dispersion model for studying the nonleaky first stop band herein is modified from the Kazarinov and Henry (KH) model which employs the zeroth, first, and second Fourier harmonics of the dielectric constant modulation [16]. The KH model describes well the dynamics of the second stop band of weakly modulated photonic lattices as verified by rigorous calculation in many cases [7,17].

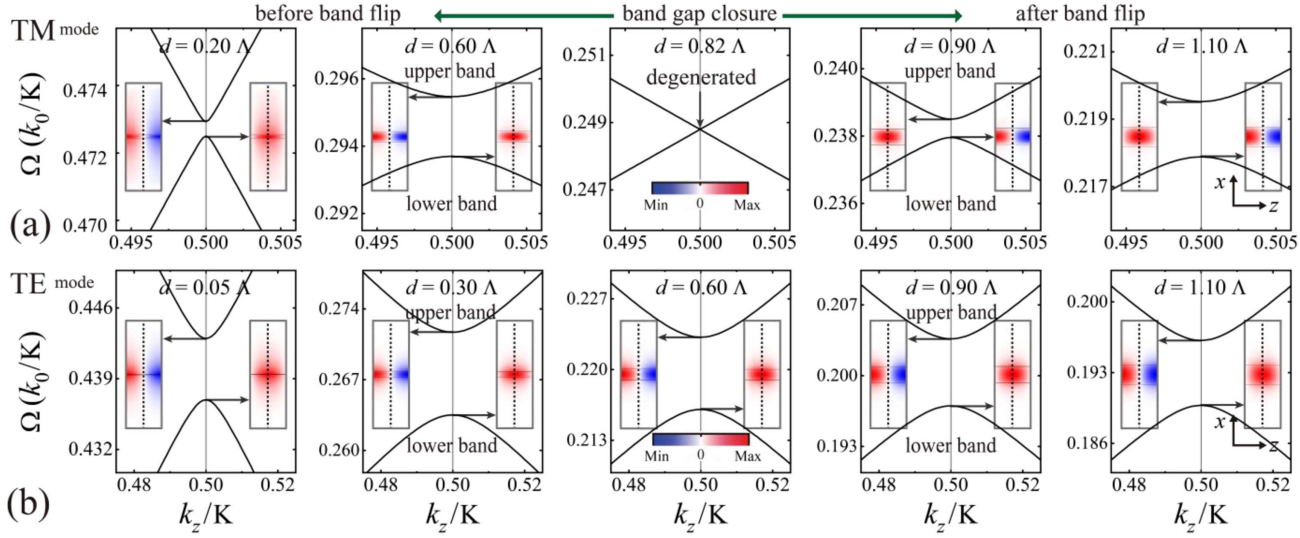

Fig. 2. (a) FDTD simulated dispersion relations near the first TM band gap for five different values of d. Here, the normalized frequency $\Omega = k_0/\mathrm{K}$, where k_0 represents the free-space wavevector, is real because we are investing the nonleaky first stop bands. The band gap closes when $d = 0.82\Lambda$. Insets represent the spatial magnetic field (H_y) distributions of band edge modes. Before and after the band gap closure, spatial field profiles of the band edge modes flip. (b) Simulated dispersion relations near the first TE band gap. Insets represent spatial electric field (E_y) distributions of band edge modes. There is neither band gap closure nor band flip. In the FDTD simulations, we use structural parameters $\rho = 0.40$, $\varepsilon_s = 1.00$, $\varepsilon_{\mathrm{avg}} = 9.00$, and $\Delta\varepsilon = 1.00$. The size of a computational cell is $\Delta x \times \Delta z = \Lambda \times 8\Lambda$ and spatial resolution is set to $\Delta x = \Delta z = 0.01\Lambda$.

We expect that our dispersion model is valid in the first stop band because higher order harmonics $\varepsilon_{n\geq 2}(x) \times \cos(n\mathrm{K}z)$ and $\xi_{n\geq 2}(x) \times \cos(n\mathrm{K}z)$ cannot contribute appreciably to the first ($q = 1$) TE and TM band gaps [17]. For convenience, in this study, we use the same geometric configuration and coordinate system used in a previous study [18].

Solving Eqs. (1) and (2) with the approximated field distributions and dielectric functions, we obtain two coupled equations

$$[\Delta\Omega \cdot (\mathrm{K}h_0) - \Delta k_z/2]A + h_1 B = 0, \tag{7}$$

$$[\Delta\Omega \cdot (\mathrm{K}h_0) + \Delta k_z/2]B + h_1 A = 0, \tag{8}$$

where $\Delta\Omega$ represents the deviation from the Bragg frequency Ω_0 under vanishing index modulation ($\varepsilon_h \sim \varepsilon_l$) [7,17,18]; Δk_z is the wavevector deviation from X, and h_0 and h_1 represent the coupling coefficients associated with the zeroth and first Fourier harmonics. Details of the mathematical process to obtain Eqs. (7) and (8) are provided in Appendix A. From Eqs. (7) and (8), near the first band edges, dispersion relations can be written as

$$\Omega(k_z) = \Omega_0 \pm \sqrt{h_1^2 + (\mathrm{X} - k_z)^2/4}/(\mathrm{K}h_0). \tag{9}$$

We note that Eqs. (7)–(9) are valid for both TE and TM modes with different coupling coefficients given by

$$h_0^{\mathrm{TE}} = \Omega \int_{-\infty}^{\infty} \varepsilon_0(x)\varphi_{\mathrm{TE}}(x)\varphi_{\mathrm{TE}}^*(x)\mathrm{d}x, \tag{10}$$

$$h_1^{\mathrm{TE}} = \frac{\Omega^2\mathrm{K}}{4} \int_{-d}^{0} \varepsilon_1(x)\varphi_{\mathrm{TE}}(x)\varphi_{\mathrm{TE}}^*(x)\mathrm{d}x, \tag{11}$$

$$h_0^{\mathrm{TM}} = \Omega \int_{-\infty}^{\infty} \varphi_{\mathrm{TM}}(x)\varphi_{\mathrm{TM}}^*(x)\mathrm{d}x, \tag{12}$$

$$h_1^{\mathrm{TM}} = \frac{1}{4\mathrm{K}} \int_{-d}^{0} \xi_1(x) \left(\mathrm{X}^2 \varphi_{\mathrm{TM}}(x)\varphi_{\mathrm{TM}}^*(x) - \frac{d\varphi_{\mathrm{TM}}(x)}{dx}\frac{d\varphi_{\mathrm{TM}}^*(x)}{dx} \right) \mathrm{d}x. \tag{13}$$

Equation (9) indicates that the first TE and TM band gaps with two band edges $\Omega^s = \Omega_0 - h_1/(\mathrm{K}h_0)$ and $\Omega^a = \Omega_0 + h_1/(\mathrm{K}h_0)$ open at $k_z = \mathrm{X}$. As displayed in Eqs. (7) and (8), one band edge mode with Ω^s is obtained when the field distribution is a symmetric cosine function ($A = B$), and the other band edge mode with Ω^a is obtained when the field distribution is an asymmetric sine function ($A = -B$). Because the relative position of the two band edge modes as well as the size of the TE and TM band gaps are directly associated with the coupling coefficients presented in Eqs. (10)–(13), different dynamics of TE and TM band gaps shown in Fig. 2 can be understood by investigating the coupling coefficients. Figures 3(a)–3(d) illustrate numerically calculated coupling coefficients h_0^{TE}, h_1^{TE}, h_0^{TM}, and h_1^{TM}, respectively, as a function of d. As shown in Figs. 3(a) and 3(b), values of h_0^{TE} and h_1^{TE} are positive irrespective of d. Hence, the symmetric band edge mode with frequency Ω^s should locate below the asymmetric band edge mode with Ω^a. In the case of the TM mode, on the other hand, Figs. 3(c) and 3(d) show that the sign of h_1^{TM} changes once from positive to negative when $d = 0.827\Lambda$, whereas h_0^{TM} is positive irrespective of d. Therefore, the relative position of the band edge modes changes with the sign change

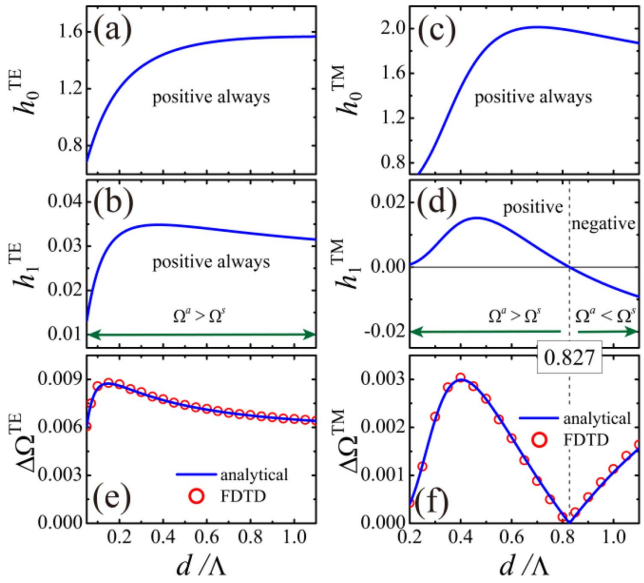

Fig. 3. Numerically calculated coefficients (a) h_0^{TE}, (b) h_1^{TE}, (c) h_0^{TM}, and (d) h_1^{TM} as functions of d. Lattice parameters are the same as in Fig. 2. The sign of h_1^{TM} changes once from positive to negative when $d = 0.827\Lambda$, whereas coefficients h_0^{TE}, h_1^{TE}, and h_0^{TM} are positive irrespective of d. The sizes of (e) TE band gap, and (f) TM band gaps obtained from our semianalytical dispersion model and FDTD simulations agree well.

of h_1^{TM}. When the value of h_1^{TM} is positive (negative), the symmetric mode with Ω^s locates below (above) the asymmetric mode with Ω^a.

To check the validity of our semianalytical dispersion model, we next investigate band gap size as a function of d. In Figs. 3(e) and 3(f), blue lines and red circles represent the size of the first band gaps obtained from the semianalytical model and FDTD simulations, respectively. As the thickness increases, as shown in Fig. 3(e), the size of the TE band gap $\Delta\Omega^{\mathrm{TE}}$ increases and reaches a maximal value when $d = 0.148\Lambda$. The gap size monotonically decreases as d is further increased. On the other hand, Fig. 3(f) shows that as the thickness increases the size of the TM band gap $\Delta\Omega^{\mathrm{TM}}$ increases, reaches a maximal value when $d = 0.402\Lambda$, decreases, and becomes zero when $d = 0.827\Lambda$ with $h_1^{\mathrm{TM}} = 0$. On additional increases in d, the TM band gap reopens, and its size increases again. We can verify that a band flip takes place with band closure when $d = 0.827\Lambda$. In Figs. 3(e) and 3(f), the solid blue lines calculated from the dispersion model with only the zeroth and first-order Fourier harmonics agree well with the red circles obtained from FDTD simulations with a nonapproximated lattice.

The sign of the coupling coefficients h_0^{TE}, h_1^{TE}, and h_0^{TM} can be understood from the guided-mode profiles $\varphi_{\mathrm{TE}}(x)$ and $\varphi_{\mathrm{TM}}(x)$ and the Fourier coefficients of the dielectric constant modulation $\varepsilon_0(x)$ and $\varepsilon_1(x)$. Because the transverse profiles for TE and TM guided modes are real functions, $\varphi_{\mathrm{TE}}(x)\varphi_{\mathrm{TE}}^*(x) = |\varphi_{\mathrm{TE}}(x)|^2$ and $\varphi_{\mathrm{TM}}(x)\varphi_{\mathrm{TM}}^*(x) = |\varphi_{\mathrm{TM}}(x)|^2$ are non-negative in $x \in [-\infty, \infty]$. Hence, h_0^{TM} in Eq. (12) is positive irrespective of d. Coefficients h_0^{TE} in Eq. (10) and h_1^{TE} in Eq. (11) are also positive because $\varepsilon_0(x)$ and $\varepsilon_1(x)$ are positive in the ranges of integration $[-\infty, \infty]$, and $[-d, 0]$, respectively. On the other hand, from Eq. (13) it is demonstrated

that the sign of h_1^{TM} is determined by the competition of two different terms $h_{1,1}^{\mathrm{TM}} = (1/4\mathrm{K})\int \xi_1(x)\mathrm{X}^2|\varphi_{\mathrm{TM}}(x)|^2 dx$ and $h_{1,2}^{\mathrm{TM}} = -(1/4\mathrm{K})\int \xi_1(x)|d\varphi_{\mathrm{TM}}(x)/dx|^2 dx$. Because $\xi_1(x)$ is negative when $x \in [-d, 0]$, $h_{1,1}^{\mathrm{TM}}$ is negative, and $h_{1,2}^{\mathrm{TM}}$ is positive irrespective of d. Hence, $h_{1,1}^{\mathrm{TM}}(h_{1,2}^{\mathrm{TM}})$ tends to locate the symmetric band edge mode with Ω^s above (below) the asymmetric mode with Ω^a. The coefficient $h_{1,1}^{\mathrm{TM}}$ can be considered to represent the Bragg effect induced by the periodic modulation of the dielectric function in the z direction because $h_{1,1}^{\mathrm{TM}}$ originates from the second derivative term $\partial[\xi(x,z)\cdot(\partial H_y/\partial z)]/\partial z$ in Eq. (2). Similarly, the coefficient $h_{1,2}^{\mathrm{TM}}$ originates in the discontinuity of the dielectric constant at the surfaces of thin-film geometry in the x direction because $h_{1,2}^{\mathrm{TM}}$ comes from the first derivative term $\partial[\xi(x,z)\cdot(\partial H_y/\partial x)]/\partial x$ in Eq. (2). Because h_1^{TE} originates in only the in-plane index modulation by means of the second derivative term $\partial^2 E_y/\partial z^2$ in Eq. (1), we conclude reasonably that TE and TM band gaps are different because only the TM gaps are affected by the discontinuity of the dielectric constant at the interfaces of the photonic lattice.

In summary, we treat the first Bragg TE and TM band gaps of 1D thin-film photonic lattices through a semianalytical dispersion model and FDTD simulations. With clear understanding rooted in the semianalytical model, we show that the TM band gaps are governed by the discontinuity of the dielectric constant at the interfaces of the photonic lattice as well as by the periodic in-plane dielectric constant modulation. The TM band gap closes when these two different effects cancel each other out as in Eq. (13). Moreover, we verify TM band flips wherein the modal profiles of the band edge modes are reversed. In contrast, the TE band gaps are formed only by in-plane coupling caused by index modulation and thus exhibit no band closure. Our research is limited here to the first stop band of the simplest 1D lattice. However, extension of this work to higher-order stop bands and to 2D lattices is feasible. This contribution may lead to deepened understanding of the properties of the band structure and band dynamics of 1D and 2D photonic lattices.

APPENDIX A: COUPLED EQUATIONS IN EQS. (7) AND (8)

Here, we provide the mathematical process to obtain Eqs. (7) and (8). Substituting Eqs. (4) and (6) into Eq. (2) and collecting terms with $\exp(+i\mathrm{X}z)$ and $\exp(-i\mathrm{X}z)$, we obtain two coupled equations for TM mode given by

$$\left[\frac{\partial}{\partial x}\left(\xi_0\frac{\partial}{\partial x}\right) - \mathrm{X}^2\xi_0 + (\mathrm{K}\Omega)^2 - \Delta k_z \mathrm{K}\xi_0\right]A\varphi_{\mathrm{TM}}(x) + \frac{1}{2}\left[\mathrm{X}^2\xi_1 + \frac{\partial}{\partial x}\left(\xi_1\frac{\partial}{\partial x}\right)\right]B\varphi_{\mathrm{TM}}(x) = 0, \tag{A1}$$

$$\left[\frac{\partial}{\partial x}\left(\xi_0\frac{\partial}{\partial x}\right) - \mathrm{X}^2\xi_0 + (\mathrm{K}\Omega)^2 + \Delta k_z \mathrm{K}\xi_0\right]B\varphi_{\mathrm{TM}}(x) + \frac{1}{2}\left[\mathrm{X}^2\xi_1 + \frac{\partial}{\partial x}\left(\xi_1\frac{\partial}{\partial x}\right)\right]A\varphi_{\mathrm{TM}}(x) = 0. \tag{A2}$$

Assuming that $A(z) = A\exp(i\Delta k_z z)$ and $B(z) = B\exp(i\Delta k_z z)$ are slowly varying, where $\Delta k_z = k_z - \mathrm{X}$, the second-order derivative terms $\partial^2 A(z)/\partial z^2$ and $\partial^2 B(z)/\partial z^2$ have been dropped in Eqs. (A1) and (A2). Because $\varphi_{\mathrm{TM}}(x)\exp(+i\mathrm{X}z)$ is the homogeneous solution of Eq. (2) at the Bragg frequency Ω_0 (center of stop band), the following equation holds:

$$\left[\frac{\partial}{\partial x}\left(\xi_0\frac{\partial}{\partial x}\right) - \mathrm{X}^2\xi_0 + (\mathrm{K}\Omega_0)^2\right]\varphi_{\mathrm{TM}}(x) = 0. \tag{A3}$$

Substituting Eq. (A3) into Eqs. (A1) and (A2) and applying the relation $\Delta\Omega = \Omega - \Omega_0 \approx (\Omega^2 - \Omega_0^2)/(2\Omega)$, we obtain

$$\left[(\Delta\Omega\cdot\mathrm{K})\Omega - \frac{\Delta k_z}{2}\xi_0\right]A\varphi_{\mathrm{TM}}(x) + \frac{1}{4\mathrm{K}}\left[\mathrm{X}^2\xi_1 + \frac{\partial}{\partial x}\left(\xi_1\frac{\partial}{\partial x}\right)\right]B\varphi_{\mathrm{TM}}(x) = 0, \tag{A4}$$

$$\left[(\Delta\Omega\cdot\mathrm{K})\Omega + \frac{\Delta k_z}{2}\xi_0\right]B\varphi_{\mathrm{TM}}(x) + \frac{1}{4\mathrm{K}}\left[\mathrm{X}^2\xi_1 + \frac{\partial}{\partial x}\left(\xi_1\frac{\partial}{\partial x}\right)\right]A\varphi_{\mathrm{TM}}(x) = 0. \tag{A5}$$

Equations (7) and (8) are obtained by multiplying Eqs. (A4) and (A5) with $\varphi_{\mathrm{TM}}^*(x)$ and integrating in the range $-\infty < x < \infty$. Here, the mode profile is normalized as $\int \xi_0(x)|\varphi_{\mathrm{TM}}(x)|^2 dx = 1$. We can also obtain Eqs. (7) and (8) for the TE mode by substituting Eqs. (3) and (5) into Eq. (1) and following the same procedure. For TE modes, normalization condition is $\int |\varphi_{\mathrm{TE}}(x)|^2 dx = 1$.

Funding. National Science Foundation (ECCS-1809143).

REFERENCES

1. Y. A. Vlasov, M. O'Boyle, H. F. Hamann, and S. J. McNab, Nature **438**, 65 (2005).
2. S. G. Johnson, P. R. Villeneuve, S. Fan, and J. D. Joannopoulos, Phys. Rev. B **62**, 8212 (2000).
3. K. Hirose, Y. Liang, Y. Kurosaka, A. Watanabe, T. Sugiyama, and S. Noda, Nat. Photonics **8**, 406 (2014).
4. A. Kodigala, T. Lepetit, Q. Gu, B. Bahari, Y. Fainman, and B. Kanté, Nature **541**, 196 (2017).
5. R. Magnusson, Opt. Lett. **39**, 4337 (2014).
6. M. J. Uddin, T. Khaleque, and R. Magnusson, Opt. Express **22**, 12307 (2014).
7. Y. Ding and R. Magnusson, Opt. Express **15**, 680 (2007).
8. E. Chow, S. Y. Lin, S. G. Jonhson, P. R. Villeneuve, J. D. Joannopoulos, J. R. Wendt, G. A. Vawter, W. Zubrzycki, H. Hou, and A. Alleman, Nature **407**, 983 (2000).
9. S. S. Wang and R. Magnusson, Appl. Opt. **32**, 2606 (1993).
10. S. G. Lee, S. Y. Jung, H. S. Kim, S. Lee, and J. M. Park, Opt. Lett. **40**, 4241 (2015).
11. J. D. Joannopoulos, R. D. Meade, and J. N. Winn, *Photonic Crystals: Molding the Flow of Light* (Princeton University Press, 1995).
12. A. F. Oskooi, D. Roundy, M. Ibanescu, P. Bermel, J. D. Joannopoulos, and S. G. Johnson, Comput. Phys. Commun. **181**, 687 (2010).
13. R. Magnusson and M. Shokooh-Saremi, Opt. Express **16**, 3456 (2008).
14. D. Rosenblatt, A. Sharon, and A. A. Friesem, IEEE J. Quantum Electron. **33**, 2038 (1997).
15. W. Streifer, D. R. Scifres, and R. D. Burnham, IEEE J. Quantum Electron. **12**, 74 (1976).
16. R. F. Kazarinov and C. H. Henry, IEEE J. Quantum Electron. **21**, 144 (1985).
17. S.-G. Lee and R. Magnusson, Phys. Rev. B **99**, 045304 (2019).
18. S.-G. Lee and R. Magnusson, Opt. Express **27**, 18180 (2019).